Eur Spine J (2015) 24:1729–1737
DOI 10.1007/s00586-015-3851-z

ORIGINAL ARTICLE

Differentiation of tuberculosis and metastatic cancer in the spine using dynamic contrast-enhanced MRI

Ning Lang · Min-Ying Su · Hon J. Yu · Huishu Yuan

Received: 22 October 2014 / Revised: 17 January 2015 / Accepted: 26 February 2015 / Published online: 8 March 2015

Abstract
Purpose To investigate the differences between imaging features of spinal tuberculosis (TB) and metastatic cancer measured by dynamic contrast-enhanced magnetic resonance imaging (DCE-MRI). The presentation of TB on convention MRI may not show the typical TB signs, and they may be mis-diagnosed as malignant diseases. DCE-MRI may provide additional information to help making differential diagnosis.
Materials and methods DCE-MRI was performed in 24 TB and 22 metastatic cancer patients. The DCE kinetic pattern was determined as "wash-out", "plateau" or "persistent enhancement". The characteristic DCE parameters were calculated from the signal intensity time course. The two-compartmental pharmacokinetic model was used to obtain K^{trans}, which is the parameter associated with the delivery of MR contrast agents into the lesion, and k_{ep}, which is the parameter associated with the distribution and clearance of contrast agents from the lesion.
Results Of the 24 TB, one case showed the wash-out kinetic pattern, 12 cases showed the plateau pattern, and 11 cases showed the persistent enhancement pattern. Of the 22 metastatic cancers, 12 cases showed wash-out, 7 cases showed plateau, and 3 cases showed persistent enhancement patterns. Compared to the metastatic cancer group, the TB group had a lower k_{ep} (0.27 ± 0.15 vs. 0.49 ± 0.23 min^{-1}, $P < 0.001$). The ROC analysis showed that the area under the curve was 0.780 for k_{ep}.
Conclusions DCE-MRI may provide additional information for differentiation between spinal TB and metastasis, when their manifestations on conventional imaging were similar.

Keywords Tuberculosis · Metastatic cancer · Spine · Dynamic contrast-enhanced MRI · Differential diagnosis

Introduction

Metastatic cancer and spinal tuberculosis (TB) are commonly diagnosed lesions in the spine. Bone metastases from various primary cancers are frequently seen in clinic, and the spines are one of the easiest body sites to be affected. Spinal tuberculosis is a common benign disease, usually endemic especially in developing countries, and the incidence of spinal tuberculosis ranks top in tuberculosis of bones and joints. When the typical signs of TB are not developed, the clinical manifestations can be very similar to metastasis and cannot be easily differentiated. Also, they may cause similar symptoms to patients, mostly pain. Because these two diseases require very different treatments, the correct preoperative diagnostic imaging would tremendously help the determination of the suitable

This work was supported in part by a research grant R01 CA 127927 from the National Institute of Health in the United States and the National Natural Science Foundation of China (81471634).

N. Lang · H. Yuan (✉)
Department of Radiology, Peking University Third Hospital, 49 North Garden Road, Haidian District, Beijing 100191, People's Republic of China
e-mail: huishuy@bjmu.edu.cn

N. Lang
e-mail: langning800129@126.com

M.-Y. Su (✉) · H. J. Yu
Department of Radiological Sciences, Tu and Yuen Center for Functional Onco-Imaging, University of California, 164 Irvine Hall, Irvine, CA 92697-5020, USA
e-mail: msu@uci.edu

procedures to be performed next and the optimal treatment methods [1–3].

The vertebral fractures, soft tissue mass and spinal canal involvement can cause radiating pain, paresthesia, limb weakness (or paralysis) and other symptoms induced by nerve root or spinal cord compression. Both spinal tuberculosis and metastases showed vertebral bone destruction and local mass on the imaging examination, and they could be solitary or multiple. The typical manifestations of spinal tuberculosis are vertebral bone destruction, narrowing of intervertebral disk space and paraspinal abscess; while the manifestations of the spinal metastases mainly are vertebral bone destruction and soft tissue mass, but disc affection is rare. If a TB lesion shows typical features, the differential diagnosis is relatively easy. However, if the patient who comes for examination has the lesion in a developmental stage when the tuberculous abscess has not yet formed or when the tuberculosis has not involved the intervertebral disk, the paraspinal lesion appears as a solid mass, and it will be very difficult to be distinguished from soft metastatic mass.

Magnetic resonance imaging (MRI) is the most useful imaging modality for diagnosing lesions in the spine. Administration of gadolinium [Gd] MR contrast agents is needed as a routine procedure to acquire images before and after contrast injection. It was found that the signal intensity of lesions (pre- or post-Gd), peritumor edema, and vessels and nerves surrounding tumors shown on conventional MRI is not specific to differentiate between benign and malignant spinal lesions or among different types of malignant lesions [4–9]. In the spine, dynamic contrast-enhanced MRI (DCE-MRI) has been applied to characterize the normal bone marrow and hematological malignancy of different origins and grades/stages [10–14]. The main difference between conventional MRI and DCE-MRI is the number of images that are acquired after contrast injection. In conventional MRI, usually only one set of post-contrast images is acquired at several minutes after [Gd] injection. In DCE-MRI, continuous imaging is performed to acquire multiple sets of images before and after [Gd] injection, which can be used to measure a signal intensity curve at different time points before and after injection. This curve is usually referred to as the DCE kinetics, which can be analyzed to reveal the delivery of [Gd] contrast agents to the lesion, as well as the distribution and clearance of [Gd] from the lesion. These DCE features are related to the vascular and cellular properties of lesions and can provide additional information for diagnosis [15].

Tumors need angiogenesis to sustain rapid growth. These new vessels are immature and leakier (i.e., they have wider endothelial junctions), which allow contrast agents to quickly leak from the vascular space into the interstitial space and diffuse back into the vascular space for clearance [16]. DCE-MRI can be used to measure the transport kinetics of contrast agents in the tissue and obtain parameters associated with vascular perfusion, volume and permeability [17–19]. In a prior study, we have shown that DCE-MRI could differentiate between myeloma and metastatic cancer in the spine [15]. So far, there is no report for differentiating between tuberculosis and metastatic cancer.

In this study, we measured the contrast enhancement time course of TB and metastatic cancers and compared the DCE kinetics between these two groups. In addition to evaluating the pattern of DCE curves, the heuristic analysis method and pharmacokinetic model fitting were applied to measure the peak and the steepest wash-in enhancements, as well as K^{trans} and k_{ep}. The ability of these parameters to differentiate between TB and metastatic cancer groups was assessed using the receiver operating characteristic (ROC) analysis to investigate how the DCE-MRI can be used to differentiate between these two commonly seen lesions in the spine.

Materials and methods

Patients

This was a retrospective study. Patients who had MRI examinations that included a DCE sequence and were confirmed as TB or metastatic cancers were identified for analysis. A total of 24 tuberculosis cases and 22 metastatic cancer cases were found between June 2008 and June 2012. No metastatic patient has TB and also no TB patient has any sign of malignant cancer. All patients were suspected to have lesions compressing the spinal cord that caused symptoms and were referred to receive an MRI examination for diagnosis. Of the 24 TB patients (15 male, 9 female, age 43 ± 18 years old), 22 patients had multiple lesions and 2 patients had a single lesion. Of the 22 patients with metastatic cancer (13 male, 9 female, age 55 ± 13 years old), 17 patients had multiple lesions and 5 patients had a single lesion. This study was approved by the Medicinal Ethics Committee of the Peking University Third Hospital.

In 22 metastatic carcinoma patients, 3 patients went to hospital because of numbness and weakness of extremities in innervation area of nerves in bone destruction segments, and 19 patients had local pain in lesion site. Five patients had a known diagnosis of primary cancer before, and because of this history, they were suspected to have metastasis to the spine. The remaining 17 patients did not have cancer history. Biopsy of the detected spinal lesion was performed in all patients to obtain pathological diagnosis, and six patients received surgery later so they also had

confirmation from surgical pathology. The primary cancers were lung cancer (seven cases), thyroid cancer (five cases), liver cancer (four cases), breast cancer (three cases), kidney cancer (two cases), and prostate cancer (one case).

In 24 tuberculosis patients, 1 patient went to hospital because of abdominal discomfort, and the other 23 patients had local pain in lesion site. The TB pathology was confirmed by biopsy of the detected spinal lesion in 21 patients. Three TB patients were given TB treatment without biopsy, and the diagnosis of TB was confirmed based on the good response to the TB treatment. The fact that most patients had no obvious primary cancer history or tuberculosis history in other sites, combined with their similar clinical symptoms, made clinical diagnosis to differentiate between mets and TB very difficult.

Study methods have been published previously [15]. Details of MR protocol, image analysis to measure DCE kinetics, analysis of characteristic DCE parameters, analysis of quantitative parameters using pharmacokinetic modeling and statistical analysis were described there. A brief summary was given below.

MRI protocol

MR scans were performed on a 3T scanner (Trio; Siemens, Erlangen, Germany). The imaging protocol included transversal T2-weighted imaging (T2WI), sagittal T2WI with and without fat suppression, and sagittal T1-weighted imaging (T1WI). After the abnormal region was identified, DCE-MRI was performed using the three-dimensional volume interpolated breath-hold examination (3D VIBE) sequence in the transversal plane to further examine that region. The scan parameters were set to repetition time = 4.1 ms, echo time = 1.5 ms, flip angle = 10°, acquisition matrix = 256 × 192 and field of view = 250 × 250 mm. Approximately, 30 slices with 3-mm thickness were prescribed to cover the abnormal vertebrae. The temporal resolution varied from 10 to 14 s. The contrast agent, 0.2 mmol/kg Gd-DTPA, was injected after one set of precontrast images was acquired using an Ulrich power injector at a rate of 2 ml/s followed by a 20-cc saline flush at the same rate. A total of 12 frames were acquired, so the total DCE-MRI acquisition time ranged from 120 to 168 s.

Image analysis to measure DCE kinetics

Images were reviewed by two radiologists (NL and HY) with 11 and 22 years of experience in diagnosis of spine diseases on MRI. The area showing the highest enhancement on one imaging slice was selected as the region of interest (ROI) by manual drawing. The ROI size was from 0.5 to 1 cm^2, and caution was taken to exclude cysts, calcification, necrosis, and hemorrhage. For each case, the junior radiologist placed the ROI, and then the senior radiologist reviewed them and confirmed that the ROI was placed in an appropriate location. Since the purpose of this study was focused on the analysis of DCE kinetics, the features on conventional MRI were not systematically analyzed and reported here.

The signal intensity time course from the ROI was measured using the Siemens Sygno Mean Curve software. For each DCE kinetic curve, there are several important features that can be analyzed. The wash-in phase is referring to the increase of signal intensity within the first minute after injection of [Gd] contrast agents, which reveals the amount of [Gd] delivered into the lesion by blood perfusion. The peak enhancement is referring to the maximum signal intensity in the DCE kinetic curve, which indicates the highest amount of [Gd] contrast agents that are delivered and retained in the lesion at one post-Gd time point. Another important feature is the delayed phase after the peak point or after 1-min after injection, and it is usually classified into three DCE kinetic patterns based on the change of signal from the peak or the 1-min time point to the last time point: (1) the wash-out pattern: the signal intensity reaches a peak before 1-min after injection, and shows wash-out with greater than 10 % decrease from the peak intensity; (2) the plateau pattern: the signal intensity does not reach a clear peak before 1-min after injection, and shows a plateau phase with smaller than 10 % change from the 1-min intensity; and (3) the persistent enhancement pattern: the signal intensity continues to enhance during the entire DCE period with greater than 10 % increase from the 1-min intensity. Figures 1, 2 and 3 illustrate 3 TB cases showing the wash-out, plateau, and persistent enhancement patterns, respectively.

Analysis of characteristic DCE parameters

Several characteristic parameters can be extracted based on the enhancement time course. The maximum signal intensity from all measured time points is identified, and that is used to calculate the peak enhancement using Eq. (1) by normalizing to the pre-contrast signal intensity.

$$\text{Peak SE}\% = \left[(\text{SI}_{\text{peak}} - \text{SI}_{\text{initial}})/\ \text{SI}_{\text{initial}}\right] \times 100\ \% \quad (1)$$

where SI_{peak} is the signal intensity at the peak time point (or the intensity at the last time point for those showing the persistent enhancement pattern), and $\text{SI}_{\text{initial}}$ is the pre-contrast signal intensity before injection. Next, the steepest wash-in segment during the ascending phase was determined by identifying the two adjacent time points that show the largest increase in signal intensity. The enhancement over the baseline SI was calculated as the Steepest Wash-in SE% using Eq. (2).

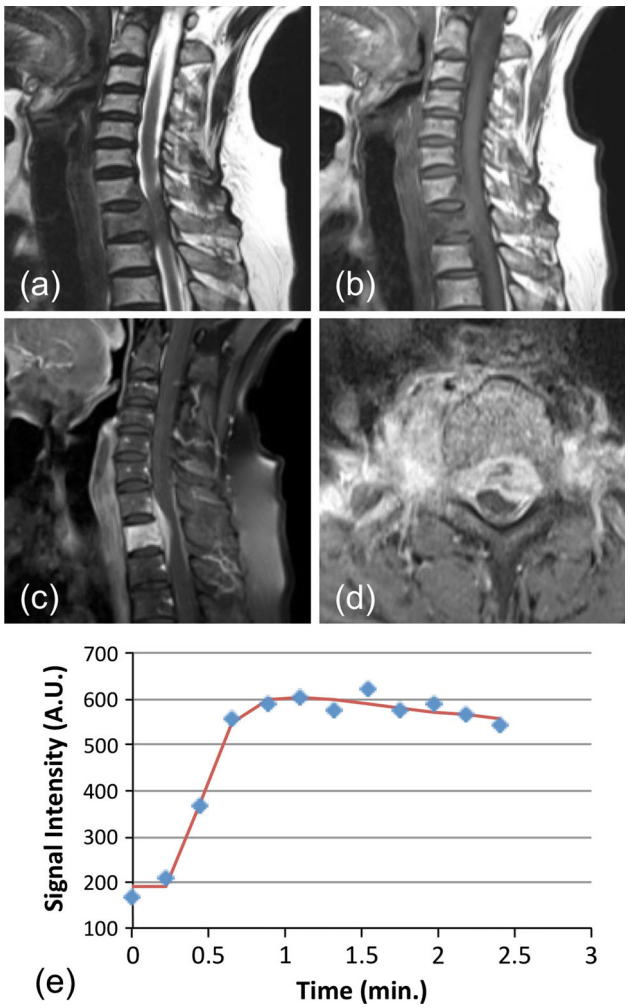

Fig. 1 A 64-year-old male patient with confirmed pathological diagnosis as tuberculosis. **a** MR T2WI and **b** MR T1WI show steolytic destruction in C7-T1 vertebral body. A soft tissue mass compressing the spinal canal is shown and the vertebra disc is not affected. **c**, **d** Contrast-enhanced MR T1WI shows a heterogeneously enhanced lesion. **e** The DCE kinetics shows a wash-out pattern (peak around 1-min and shows 10 % decrease). In pharmacokinetic analysis, the fitted $K^{trans} = 0.117$/min, $k_{ep} = 0.499$/min

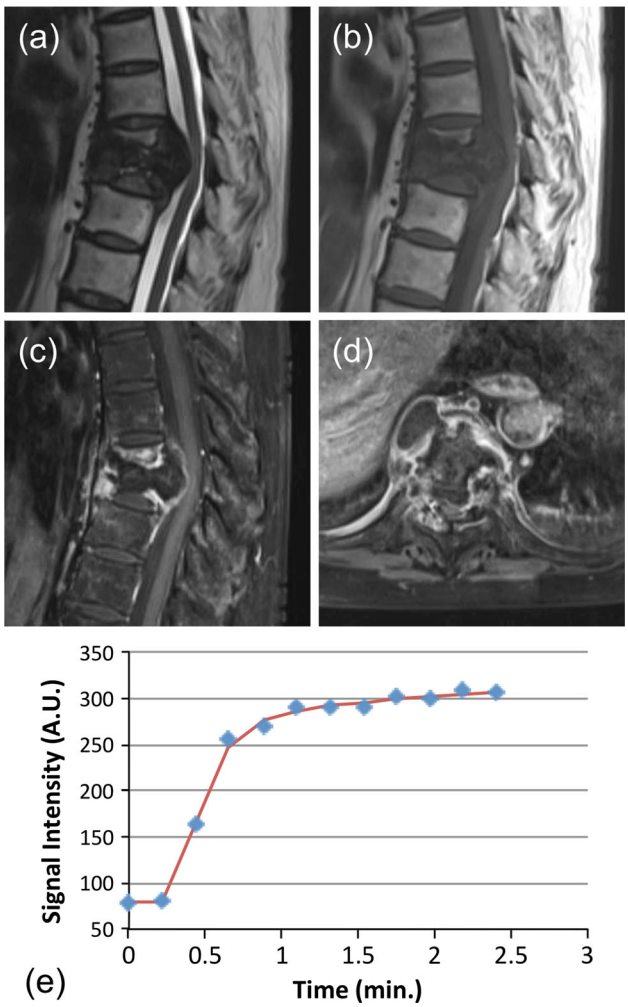

Fig. 2 A 62-year-old female patient with confirmed pathological diagnosis as tuberculosis. **a** MR T2WI and **b** MR T1WI show steolytic destruction in T7-8 vertebral body. A soft tissue mass compressing the spinal canal is shown and the vertebra disc is affected. **c**, **d** Contrast-enhanced MR T1WI shows a heterogeneously enhanced lesion. **e** The DCE kinetics shows a plateau pattern (approximately 9 % increase between the last time point and the estimated 1-min point). In pharmacokinetic analysis, the fitted $K^{trans} = 0.111$/min, $k_{ep} = 0.253$/min

$$\text{Steepest Wash-in SE}\% = [(SI_2 - SI_1)/\ SI_{initial}] \times 100\ \% \quad (2)$$

Analysis of quantitative parameters using pharmacokinetic modeling

We also applied two-compartmental pharmacokinetic modeling to analyze the quantitative parameters, including the transfer constant (K^{trans}, related to wash-in into the lesion) and the rate contrast (k_{ep}, related to distribution and clearance from the lesion), using the unified Tofts model [16, 17]. The two compartments are the vascular space and the interstitial space, with the in-flux constant K^{trans} for the contrast agents to leak from the vascular to the interstitial space, and the out-flux constant k_{ep} for them to diffuse from the interstitial space back to the vascular space. For data fitting to obtain K^{trans} and k_{ep}, we used the same blood kinetic parameters used in the commercial software syngo Tissue 4D (Siemens), which are based on the blood curves reported by Parker et al. [20]. Detailed parameters and fitting procedures have been described in [15].

Statistical analysis

The DCE pattern for each case was categorized as wash-out, plateau or persistent enhancement. The fraction of

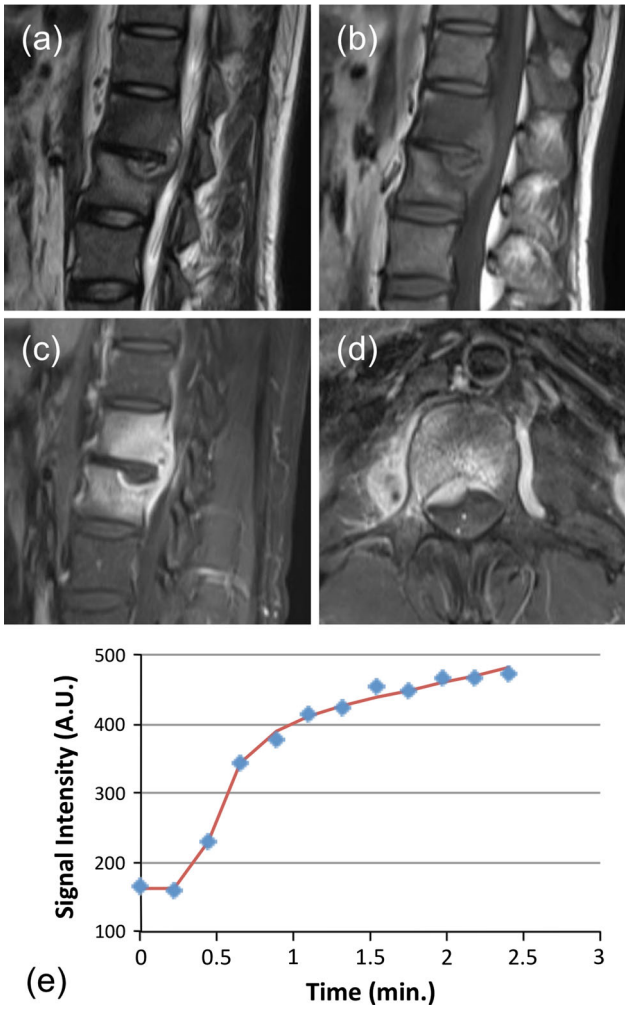

Fig. 3 A 38-year-old male patient with confirmed pathological diagnosis as tuberculosis. **a** MR T2WI and **b** MR T1WI show steolytic destruction in L1-2 vertebral body. A soft tissue mass compressing the spinal canal is shown. The narrowing of intervertebral space is noted, but the signal is not increased. **c**, **d** Contrast-enhanced MR T1WI shows a heterogeneously enhanced lesion. **e** The DCE kinetics shows a clear persistent enhancement pattern. The signal at the last time point compared to the 1-min time point shows 20 % increase. In pharmacokinetic analysis, the fitted $K^{trans} = 0.057$/min, $k_{ep} = 0.086$/min

different patterns in the TB and metastatic cancer groups was compared using the Fisher's Exact Test. The characteristic DCE parameters (peak SE%, steepest wash-in SE%) and the pharmacokinetic parameters (K^{trans} and k_{ep}) between the TB and metastatic cancer groups were compared using the two-tailed Student's t test. All analysis was performed using the SPSS 11.5 software, with $P < 0.05$ being regarded as significant. In addition, the ROC analysis was performed to evaluate the diagnostic ability of each analyzed parameter along with combined parameters (based on logistic regression) to differentiate between the TB and metastatic cancer groups.

Results

DCE kinetic patterns

Of the 24 tuberculosis, only one case (1/24 = 4 %) showed the wash-out pattern, 12 cases (12/24 = 50 %) showed the plateau pattern, and 11 cases (11/24 = 46 %) showed the persistent enhancement patterns. Of the 22 metastatic cancer cases, 12 cases (12/22 = 54 %) showed the wash-out pattern, 7 cases (7/22 = 32 %) showed the plateau pattern, and 3 cases (3/22 = 14 %) showed the persistent enhancement pattern. The portion of cases showing the wash-out DCE pattern was significantly different, 1/24 = 4 % for TB vs. 12/22 = 54 % for mets, with $p < 0.001$.

Figures 1, 2 and 3 show three examples of TB cases presenting the wash-out, plateau, and persistent enhancement patterns. Figure 4 shows a metastatic carcinoma of the renal pelvis with the wash-out DCE pattern, and Fig. 5 shows a metastatic prostate carcinoma with the wash-out DCE pattern.

DCE characteristic/pharmacokinetic parameters

The characteristic DCE parameters and the pharmacokinetic parameters in the TB and the metastatic cancer groups are summarized in Table 1. Compared to the metastatic cancer group, the TB group had a slightly higher peak SE % (198 ± 81 vs. 165 ± 60 %, $P = 0.1263$). Since most TB cases showed plateau or persistent patterns, the peak happened at a later time after 1 min, and in six cases there was no peak during the DCE period and the intensity at the last time point was used. In terms of the steepest wash-in SE % that represented the increase of intensity during the ascending phase, the TB group was slightly lower than the metastatic cancer group (100 ± 55 vs. 111 ± 41 %, $P = 0.4493$). The two groups had the same mean K^{trans} values (0.077 ± 0.036 vs. 0.077 ± 0.028, $P = 1.0000$). The rate constant k_{ep} was significantly higher in the metastatic cancer group compared to the TB group (0.49 ± 0.23 vs. 0.27 ± 0.15/min, $P < 0.001$). The parameter k_{ep} is related to the wash-out phase, and the higher value in the metastatic cancer group is consistent with more cases showing the wash-out pattern and fewer cases showing the persistent enhancement pattern.

ROC analysis

The ROC analysis was performed to differentiate between the tuberculosis and metastatic cancer groups. The area under the curve (AUC) was calculated as 0.78 for k_{ep}.

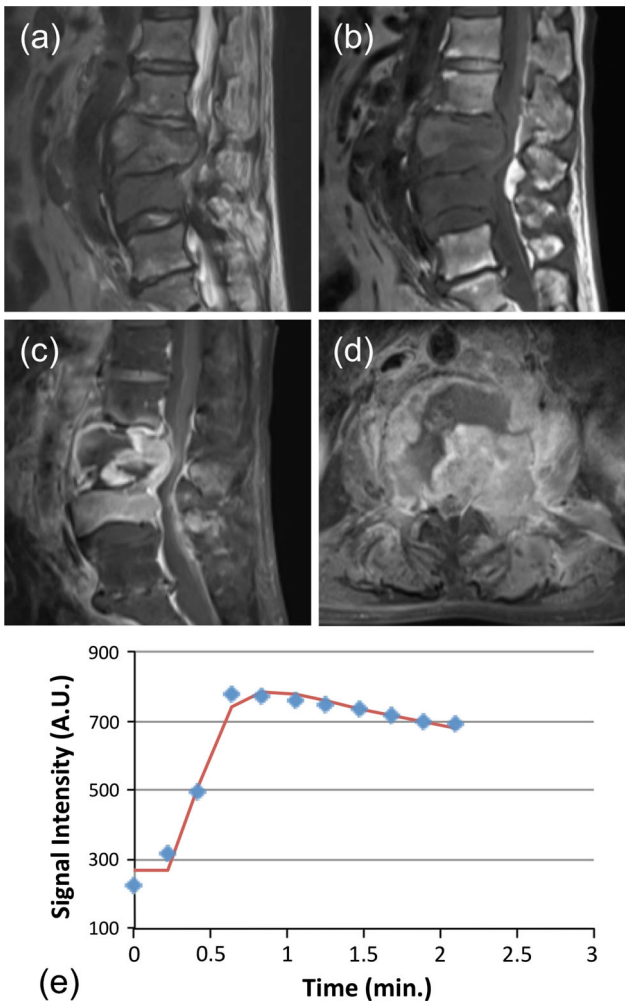

Fig. 4 A 81-year-old male patient with confirmed pathological diagnosis as metastatic cancer originated from the carcinoma of the renal pelvis. **a** MR T2WI and **b** MR T1WI show steolytic destruction in L3-4 vertebral body. A soft tissue mass compressing the vertebral body is shown. **c** and **d** Contrast-enhanced MR T1WI shows a heterogeneously enhanced lesion, and the intervertebral disc is affected. **e** The DCE kinetics shows rapid wash-in and reaches the peak at 46 s, followed by wash-out. In pharmacokinetic analysis, the fitted $K^{trans} = 0.120$/min, $k_{ep} = 0.695$/min

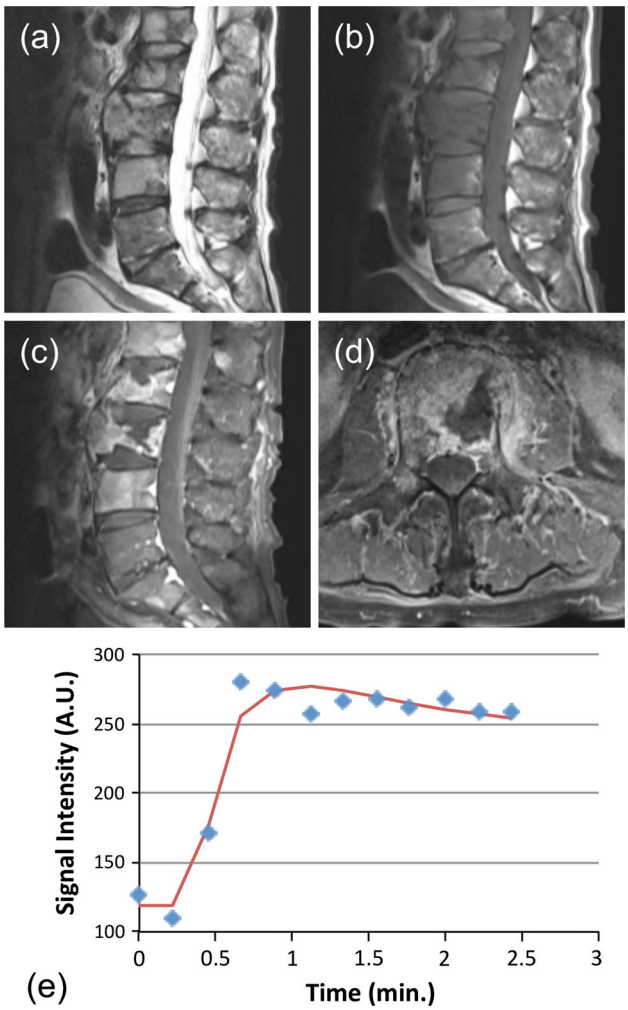

Fig. 5 A 75-year-old male patient with confirmed pathological diagnosis as metastatic cancer originated from the prostate carcinoma. **a** MR T2WI and **b** MR T1WI show steolytic destruction in L1-4 vertebral body. A soft tissue mass is clearly visible. **c**, **d** Contrast-enhanced MR T1WI shows a heterogeneously enhanced lesion. **e** The DCE kinetics shows rapid wash-in and reaches the peak after 40 s, followed by wash-out. In pharmacokinetic analysis, the fitted $K^{trans} = 0.058$/min, $k_{ep} = 0.565$/min

Discussion

Both spinal tuberculosis and metastases showed vertebral bone destruction and local mass on the imaging examination, and they could be solitary or multiple. The typical manifestations of spinal tuberculosis are vertebral bone destruction, narrowing of intervertebral disk space and paraspinal abscess. If the lesions present these typical TB signs, diagnosis is relatively easy. The manifestations of the spinal metastases are mainly vertebral bone destruction and soft tissue mass, with rare disc involvement. For TB, when the tuberculous abscess has not yet formed or when the tuberculosis has not involved the intervertebral disk, the paraspinal lesion shows as a solid mass and it may be misdiagnosed as malignant. When a lesion manifests as vertebral bone destruction, local mass, absence of disc involvement or abscess, the plain pre-contrast scan and static post-contrast enhancement will be difficult to distinguish between tuberculous granulomas and soft tissue mass of metastases [1–3]. In general, it is difficult to differentiate between benign and malignant musculoskeletal lesions in the spine [4–10]. All patients analyzed in this study presented similar symptoms of pain, which were suspected to come from compression of the spinal cord due to the presence of lesions. As shown in the illustrated cases, the imaging features of pre-contrast T1WI and T2WI and post-contrast T1WI are similar. In the early contrast-enhanced

Table 1 Quantitative parameters analyzed from DCE kinetics of the TB and metastatic cancer groups

	Peak SE%	Wash-in SE%	K^{trans} (1/min)	k_{ep} (1/min)
Tuberculosis ($N = 24$)	198 ± 81 %	100 ± 55 %	0.077 ± 0.036	0.27 ± 0.15
Metastasis ($N = 22$)	165 ± 60 %	111 ± 41 %	0.077 ± 0.028	0.49 ± 0.23
T value	1.56	0.76	−0.00	38.74
P value	0.1263	0.4493	1.0000	<0.001

All presented data are group mean ± standard deviation

images, bone destruction and soft tissue mass showing heterogeneous enhancements are the most common imaging features, which cannot be used to differentiate between TB and metastatic cancer. As the treatment options and the overall management for these two diseases are very different, a correct diagnosis based on imaging will be very helpful for choosing the most suitable subsequent procedures. For TB, anti-TB therapy is the main treatment options; for metastatic cancer, the patient may need additional imaging or workup to identify the primary cancer and the extent of metastasis for choosing the optimal treatment strategy (which may include surgery, radiation and chemotherapy).

Malignant tumors require angiogenesis to grow and invade. Angiogenic vessels are distributed abnormally, having uneven diameters and wider endothelial junctions (leakier vessels). In DCE-MRI, the kinetic time course is more likely to show the wash-out/plateau patterns. Inflammatory lesions such as tuberculosis have relatively mature vascular structure [21] and, thus, are less likely to show the wash-out pattern. Therefore, the different vascular properties may be measured by DCE-MRI for the diagnosis of vertebral lesions [22]. Overall, the metastatic cancer group showed a more aggressive type of DCE kinetics compared to the TB group. DCE-MRI has been widely used for evaluating many other types of cancers, but there has been no report yet for differentiating between TB and metastatic spinal lesions. In this study, we found that the signal intensity time curves of tuberculosis and metastases both increase rapidly during the wash-in phase and have similar K^{trans}, suggesting that both of them had abundant blood vessels as one of their pathological alterations either coming from angiogenesis or inflammation [20]. There was no significant difference in the maximum enhancement (peak SE%) or wash-in SE% between TB group and metastatic cancer group, indicating that there is no significant difference between the delivery or uptake of [Gd] contrast agents between them.

Although they showed similar features during the DCE wash-in phase, they had significantly different delayed phase as analyzed by the DCE kinetic patterns or k_{ep}, suggesting that they have different vascular permeability and distribution space in the lesion. In 24 cases of tuberculosis, only one case showed wash-out, 12 cases showed the plateau pattern, and 11 cases showed the persistent enhancement patterns. In pathology, the typical tubercle under microscopy often showed necrosis in the center, including mycobacterium tuberculosis, (largest number of) surrounded epithelioid cells, Langhans giant cells and peripheral infiltrating lymphocytes and a small number of fibroblasts proliferation, suggesting that the organizational structure of tuberculosis has more interstitial space allowing the retention of [Gd] MR contrast agents. The majority of TB cases showed the plateau and persistent enhancement patterns, and they even had a higher peak enhancement value compared to the metastatic cancer group. The presence of multiple small necrotic foci inside tuberculosis is commonly seen, and the contrast agents may leak to the necrotic space and show the continuous enhancement DCE pattern. In contrast, the DCE pattern for the metastatic cancer group is more likely to show the wash-out pattern. In histological examination, spinal metastatic cancers are likely to show a high cellular density with little interstitial space for retention of [Gd] contrast agents. Therefore, contrast agents can quickly fill up this limited space, then rapidly diffuse back to the bloodstream for clearance. Of the 22 tumors, 12 showed the wash-out pattern, 7 showed the plateau pattern, and only 3 showed the persistent enhancement pattern. The histopathological presentation of metastatic cancer can vary substantially and show diverse vascular and cellular characteristics; thus some cases showing plateau and persistent enhancement patterns are expected.

Pharmacokinetic model fitting was used to obtain the parameters K^{trans} and k_{ep}. We used the blood kinetics used in the commercial software Tissue 4D, which was based on the blood curve published by Parker et al. [20]. By choosing the same blood parameters as those used in this commercial software, our results can be easily compared to others analyzed using the same population-based blood kinetics. Consistent with the different DCE patterns, k_{ep} is significantly lower in the TB group compared to the metastatic cancer group. In the ROC analysis, the area under the curve for differentiating between these two groups was 0.78. Therefore, although DCE-MRI can obtain additional information, it is still very challenging for a

correct differential diagnosis between TB and metastatic cancers when there was no disk involvement or discernable abscess.

We have shown five case examples to illustrate the similar imaging presentations between TB and metastasis cases. The diagnosis for the TB case shown in Fig. 1 is very challenging. A paravertebral mass was presented without any classical sign of TB (no narrowing of the intervertebral space, and no abscess) and, furthermore, the DCE kinetics showed the wash-out pattern, all of these pointing to a malignancy diagnosis. Fortunately, of the 24 TB cases, this is the only case that showed the wash-out DCE pattern. Eleven of 24 TB cases showed the persistent enhancement pattern, e.g., the TB case shown in Fig. 3. Although it did not have a clear abscess, a subtle narrowing of the intervertebral space was noted. For this case, the persistent DCE pattern may be used for diagnosis of TB with a much higher confidence. Although biopsy is the ultimate way to yield a confirmed pathological diagnosis, as we have shown in this work, three patients who presented with the typical TB features were given TB treatment without going through biopsy, and the diagnosis was confirmed based on the response to the TB treatment. Therefore, it is possible that improved imaging methods can help the diagnosis and avoid biopsy (for benign diseases such as TB), or to recommend other procedures than spinal biopsy. For patients with metastatic cancer, if the radiologist has a high confidence of malignancy, subsequent imaging examinations may be performed. It may reveal the site of primary malignancy for biopsy, rather than performing the more difficult and risky spinal biopsy procedure.

One major limitation of the study is the small case number, and further studies using a larger sample size are needed to establish the role of DCE-MRI in diagnosis of spinal lesions. Also, in this work, we had focused on the DCE-MRI analysis and did not perform a full evaluation of all clinical information and other imaging features. A more thorough study considering all available information is needed to clearly demonstrate the added value of DCE-MRI in the clinical practice. As we have shown in this work, it is likely that more advanced imaging methods can be used to provide more reliable and accurate diagnosis and improve the management for patients with spinal lesions.

Conclusion

In summary, we have shown that DCE-MRI can provide additional information that cannot be obtained using the conventional MRI protocol to differentiate between TB and metastatic cancers. More cases in a larger study need to be analyzed to evaluate the diagnostic value of DCE-MRI for spinal lesions, as well as to build the diagnostic classifier and determine the optimal cutoff values of the quantitative parameters to achieve optimized sensitivity and specificity.

Conflict of interest The authors declared no conflicts of interest.

References

1. Go SW, Lee HY, Lim CH et al (2012) Atypical disseminated skeletal tuberculosis mimicking metastasis on PET-CT and MRI. Intern Med 51:2961–2965
2. Zheng CY, Liu DX, Luo SW et al (2011) Imaging presentation highly manifested as tuberculosis in a case of spinal metastatic carcinoma. Orthopedics 34:e436–e438
3. Yu Y, Wang X, Du B et al (2013) Isolated atypical spinal tuberculosis mistaken for neoplasia: case report and literature review. Eur Spine J 22:S302–S305
4. Gernaerdt MJA, Hogendoorn PCW, Bolem JL et al (2000) Cartilaginous tumors: fast contrast-enhanced MR imaging. Radiology 214:539–546
5. Moulton JS, Blebea JS, Dunco DM et al (1995) MR imaging of soft-tissue masses: diagnostic efficacy and value of distinguishing between benign and malignant lesions. Am J Roentgenol 164:1191–1199
6. Hermann G, Abdelwahab LF, Miller TT et al (1992) Tumour and tumour-like conditions of the soft tissue: magnetic resonance imaging features differentiating benign from malignant masses. Br J Radiol 65:14–20
7. May DA, Good RB, Smith DK et al (1997) MR imaging of musculoskeletal tumors and tumor mimickers with intravenous gadolinium: experiences with 242 patients. Skeletal Radiol 26:2–15
8. Elemann R, Reiser MF, Peters PE et al (1989) Musculoskeletal neoplasms: static and dynamic Gd-DTPA enhanced MR imaging. Radiology 171:767–773
9. Lang P, Honda G, Roberts T et al (1995) Musculoskeletal neoplasm: perineoplastic edema versus tumor on dynamic postcontrast MR imaging with spatial mapping of instantaneous enhancement rates. Radiology 197:831–839
10. Verstraete KL, De Deene Y, Roels H et al (1994) Benign and malignant musculoskeletal lesions: dynamic contrast-enhanced MR imaging-parametric "first-pass" images depict tissue vascularization and perfusion. Radiology 192:835–843
11. Stäbler A, Baur A, Bartl R et al (1996) Contrast enhancement and quantitative signal analysis in MR imaging of multiple myeloma: assessment of focal and diffuse growth patterns in marrow correlated with biopsies and survival rates. Am J Roentgenol 167:1029–1036
12. Baur A, Stäbler A, Bartl R et al (1997) MRI gadolinium enhancement of bone marrow: age-related changes in normals and in diffuse neoplastic infiltration. Skeletal Radiol 26:414–418
13. Zhang L, Mandel C, Yang ZY et al (2006) Tumor infiltration of bone marrow in patients with hematological malignancies: dynamic contrast-enhanced magnetic resonance imaging. Chin Med J 119:1256–1262
14. Hillengass J, Zechmann C, Bäuerle T et al (2009) Dynamic contrast-enhanced magnetic resonance imaging identifies a subgroup of patients with asymptomatic monoclonal plasma cell disease and pathologic microcirculation. Clin Cancer Res 15:3118–3125
15. Lang N, Su MY, Yu HJ et al (2013) Differentiation of myeloma and metastatic cancer in the spine using dynamic contrast enhanced MRI. Magn Reson Imaging 31:1285–1291

16. Barrett T, Brechbiel M, Bernardo M et al (2007) MRI of tumor angiogenesis. J Magn Reson Imaging 26:235–249
17. Tofts PS, Kermode AG (1991) Measurement of the blood–brain barrier permeability and leakage space using dynamic MR imaging. 1 Fundamental concepts. Magn Reson Med 17:357–367
18. Tofts PS (1997) Modeling tracer kinetics in dynamic Gd-DTPA MR imaging. J Magn Reson Imaging 7:91–101
19. Tofts PS, Brix G, Buckley DL et al (1999) Estimating kinetic parameters from dynamic contrast-enhanced T(1)-weighted MRI of a diffusable tracer: standardized quantities and symbols. J Magn Reson Imaging 10:223–232
20. Parker GJ, Roberts C, Macdonald A et al (2006) Experimentally-derived functional form for a population-averaged high-temporal-resolution arterial input function for dynamic contrast-enhanced MRI. Magn Reson Med 56:993–1000
21. Rosai Juan (2004) Rosai and Ackerman's surgical pathology. Elsevier, Philadelphia, pp 352–353
22. Tokuda O, Hayashi N, Taguchi K et al (2005) Dynamic contrast-enhanced perfusion MR imaging of diseased vertebrae: analysis of three parameters and the distribution of the time-intensity curve patterns. Skeletal Radiol 34:632–638